Earth and Space Science

RESEARCH ARTICLE
10.1029/2024EA003707

Decade-Long Ozone Profile Record From Suomi NPP OMPS Limb Profiler: Assessment of Version 2.6 Data

N. A. Kramarova[1], P. Xu[2], J. Mok[3], P. K. Bhartia[1,4], G. Jaross[1], L. Moy[3], Z. Chen[3], S. Frith[3], M. DeLand[3], D. Kahn[3], G. Labow[3], J. Li[3], E. Nyaku[3], C. Weaver[5], J. Ziemke[6], S. Davis[7], and Y. Jia[7,8]

[1]NASA GSFC, Greenbelt, MD, USA, [2]SAIC, Greenbelt, MD, USA, [3]SSAI, Lanham, MD, USA, [4]Emeritus at NASA GSFC, Greenbelt, MD, USA, [5]ESSIC, College Park, MD, USA, [6]Morgan State University, Baltimore, MD, USA, [7]NOAA Chemical Sciences Laboratory, Boulder, CO, USA, [8]Cooperative Institute for Research in Environmental Sciences, University of Colorado at Boulder, Boulder, CO, USA

Abstract We evaluate a decadal ozone profile record derived from the Suomi National Polar-orbiting Partnership (SNPP) Ozone Mapping and Profiler Suite (OMPS) Limb Profiler (LP) satellite instrument. In 2023, the OMPS LP data were re-processed with the new version 2.6 retrieval algorithm that combines measurements from the ultraviolet (UV) and visible (VIS) parts of the spectra. It employs the second order Tikhonov regularization to retrieve a single vertical ozone profile between 12.5 km (or cloud tops) and 57.5 km with a vertical resolution of about 1.9–2.5 km between 20 and 55 km. The algorithm uses radiances measured at six UV ozone-sensitive wavelengths (295, 302, 306, 312, 317, and 322 nm) paired with 353 nm, and one VIS wavelength at 606 nm combined with 510 and 675 nm to form a triplet. Each wavelength pair or triplet is used over a limited range of tangent altitudes where the sensitivity to ozone change is strongest. A new aerosol correction scheme was implemented based on a gamma-function particle size distribution. In addition, numerous calibration changes that affected ozone retrievals were applied to measured LP radiances, including updates in altitude registration, radiometric calibration, stray light, and spectral registration. The key version 2.6 enhancement is the improved stability of the LP ozone record confirmed by the reduction in relative drifts between LP ozone and correlative measurements, linked previously to a drift in the version 2.5 LP altitude registration.

Plain Language Summary The Montreal Protocol protects the Earth's ozone layer by regulating the production and usage of ozone-depleting substances. As a result of this international treaty, we expect stratospheric ozone to increase over time. A series of OMPS Limb Profilers (LP) was designed to ensure continuous spaceborne capabilities for detecting changes in the stratospheric ozone distribution over several decades. The ozone record from the first OMPS LP on board the Suomi NPP mission spans more than 12 years, from April 2012 to the present. A statistically significant positive drift in the previous version 2.5 of LP ozone data, linked to a drift in the LP altitude registration, has compromised its fitness to accurately detect ozone trends. In this paper, we introduce the new version 2.6 OMPS LP ozone data set with improved stability. We found a substantial reduction in relative drifts between LP ozone and correlative measurements. Therefore, the version 2.6 LP ozone can be used with higher confidence for monitoring and quantifying stratospheric ozone recovery.

Key Points:

- The ozone record from the first OMPS Limb Profiler that spans more than 12 years has been reprocessed with the new version 2.6 algorithm
- The key v2.6 improvement is the reduction in relative drift that was linked previously to a drift in the v2.5 LP altitude registration
- The study demonstrates the importance of continuous improvements in calibration and retrieval to ensure accuracy and stability of LP ozone

Supporting Information:

Supporting Information may be found in the online version of this article.

Correspondence to:

N. A. Kramarova,
natalya.a.kramarova@nasa.gov

Citation:

Kramarova, N. A., Xu, P., Mok, J., Bhartia, P. K., Jaross, G., Moy, L., et al. (2024). Decade-long ozone profile record from Suomi NPP OMPS Limb Profiler: Assessment of version 2.6 data. *Earth and Space Science*, *11*, e2024EA003707. https://doi.org/10.1029/2024EA003707

Received 25 APR 2024
Accepted 28 AUG 2024

1. Introduction

NASA has pioneered space-borne observations of the ozone layer by developing the Backscattered Ultraviolet (BUV) technique in the 1960s to measure total column ozone and ozone profile. The first BUV instrument, on NASA's Nimbus-4 platform, was launched more than 50 years ago in 1970. Ozone profile observations were continued with the improved Solar Backscattered Ultraviolet (SBUV) sensor on board of Nimbus-7, and then by the series of the SBUV/2 instruments flown on seven NOAA polar orbiting missions between 1984 and the 2010s.

The discovery of the Antarctic ozone hole in 1985 (e.g., Farman et al., 1985; Stolarski at el., 1986) triggered public concerns world-wide. Since that time the development of ozone measurement techniques has been guided by international agreements and public policies aimed to preserve the Earth's ozone layer. The US Clean Air Act specifically mandates NASA and NOAA to monitor the ozone layer, and the international community depends

upon these measurements for periodic assessments of the integrity of the ozone layer required under the Montreal Protocol (WMO, 2022).

Given the limited profiling capability of the SBUV/2 sensor, NOAA developed a suite of OMPS sensors for the NOAA/NASA joint National Polar-orbiting Operational Environmental Satellite System (NPOESS). In addition to a nadir mapping sensor (OMPS-NM) based on NASA's Total Ozone Mapping Spectrometer (TOMS) instrument, and a nadir profiler sensor (OMPS-NP) based on the SBUV/2 instrument, OMPS also has a limb scattering sensor (OMPS LP). OMPS LP is based on technologies developed by NASA in the 1980s and 1990s for the Shuttle Ozone Limb Sounding Experiment flown on STS-87 and STS-107 (Flittner et al., 2000; McPeters et al., 2000). Though OMPS does not measure a large suite of trace gasses that influence ozone photochemistry, it fully satisfies the public policy need to monitor the ozone layer (NASA, 2023). Space-borne observations with operational OMPS suites will extend into the next two decades.

Owing to the regulations imposed by the Montreal Protocol, the levels of anthropogenically produced chlorine and bromine compounds that destroy the ozone layer have been gradually declining since the early 2000s. Scientists found unambiguous increases of ∼1.0%–2.2% per decade in upper-stratospheric ozone over the 2000–2020 period (WMO, 2022), driven by declines in ozone-depleting substances and increases in greenhouse gasses (GHGs). Observations of the vertical ozone distribution derived from OMPS are used to evaluate the health of the ozone layer.

In this study we present and evaluate the OMPS LP version 2.6 ozone data product. Section 2 describes version 2.6 processing and documents changes in Level 1 (calibrated radiances) and Level 2 (ozone profile retrievals) algorithms. Section 3 evaluates SNPP OMPS LP profiles over a decade by comparing with Aura MLS. A summary is provided in Section 4. This study will be complemented by an upcoming comprehensive validation paper where OMPS LP will be compared with an extended set of correlative satellite and ground-based observations.

2. Ozone Mapping and Profiler Suite

2.1. OMPS Limb Profiler

OMPS was designed to provide profile and total ozone measurements (Flynn et al., 2006). SNPP OMPS, launched in October 2011, comprises three complementary ozone sensors—Limb Profiler (LP), Nadir Profiler (NP) and Nadir Mapper (NM)—that sample the same region of the atmosphere from Earth's surface to the mesosphere within minutes to measure the global ozone distribution at high spatial and vertical resolution (Kramarova et al., 2014). NOAA-20 (formerly JPSS-1) OMPS, launched in October 2017, includes only the two nadir sensors, but NOAA-21 (JPSS-2), launched in November 2022, has the Limb Profiler as well. Two more OMPS will be launched in the next decade including all three sensors on board of JPSS-3 and JPSS-4 missions. In this paper we focus on the ozone profile record derived from the SNPP OMPS LP. The operational observations with SNPP OMPS LP started in April 2012, and the record now exceeds 12 years.

The OMPS LP sensor measures solar irradiances scattered from the atmospheric limb in the ultraviolet (UV), visible (VIS), and near infrared (NIR) spectral ranges (between 290 and 1,000 nm) with variable spectral resolution that increases from about 1 nm at 290 to 30 nm at longer wavelengths near 1,000 nm. The instrument is mounted at the back of the spacecraft and collects measurements by viewing the atmospheric limb along the satellite track. The LP has a 1.85° vertical field of view (FOV) and covers 100 km, but because of spacecraft pointing variations it reliably measures scattered light between the ground and ∼80 km throughout the orbit. Scattered light is projected to a 2-dimensional Charge Coupled Device (CCD) detector. The vertical sampling of LP measurements, determined by the CCD pixel sampling, is ∼1 km, but the actual instantaneous FOV of each pixel is about 1.2 km. To avoid saturation of the CCD pixels and to capture measurements over the entire spectral and vertical range, the OMPS LP splits each vertical profile into two images: low altitude (bright) signals are measured with the small aperture, whereas the high altitude (low intensity) signals are measured with the large aperture. The full spectra from both apertures are produced every 19 s. Due to bandwidth limitations, data from all CCD pixels can not be downloaded from the instrument to the ground during the normal operations, and only a relatively small subset of pixels (the Sample Table) becomes available for the retrieval process. The downloaded pixels from the two spectra are then stitched together and mapped onto the regular spectral and vertical grids (Level 1G). The instrument has three slits separated horizontally by 4.25° (about 250 km) to increase the cross-

track coverage, but in this study, we focus only on measurements obtained from the center slit aligned with the satellite ground track.

2.2. Version 2.6 Processing

The first version of ozone profiles derived from the SNPP OMPS LP was released soon after the beginning of operational observations in April 2012 (Rault & Loughman, 2013). In July 2014 version 2 of the LP ozone profile data set was released which included corrections for the sensor pointing and simplification in the retrieval algorithm (Xu et al., 2014). Version 2.5 was released in July 2017 (Kramarova et al., 2018). Both version 2 and version 2.5 data sets have been produced using a modified version of the OMPS LP retrieval algorithm (Rault & Loughman, 2013), and their detailed descriptions and validation results are summarized by Kramarova et al. (2018). Here we present a new version 2.6 of the LP ozone profiles, released in March 2023. In this section we describe the key changes implemented in the Level 1 (Section 2.2.1) and Level 2 (Section 2.2.2) algorithms for the processing of version 2.6 data.

LP ozone retrievals are reported in daily files that contain ozone number density retrievals from the center slit only along with geolocation information and quality flags (Kramarova & DeLand, 2023). For users' convenience, with each ozone measurement we also report atmospheric pressure and temperature profiles that are derived from the Goddard Earth Observing System (GEOS) Forward Processing for Instrument Teams (FP-IT) product provided by the NASA Global Modeling Assimilation Office (GMAO) (Gelaro et al., 2017; Lucchesi, 2013). These meteorological fields are also used in the forward model calculations.

2.2.1. SNPP OMPS LP Calibration

In this section we describe instrumental calibrations applied to LP radiances in Level 1 processing. Radiometric errors and errors in sensor pointing (primarily those related to altitude registration errors) are the two main sources of errors in the limb scattering technique affecting the accuracy of retrieved ozone profiles (e.g., Flittner et al., 2000).

Two-dimensional (spectral-spatial) CCD detectors are susceptible to internally scattered stray light, that is, photons from bright parts of a scene can scatter to the CCD regions with a weaker signal. Jaross et al. (2014) describe the stray light (SL) corrections based on the pre-launch point-spread-function (PSF) measurements. Since the pre-launch corrections alone proved inadequate, empirical SL corrections were applied in addition to the PSF-based corrections starting with version 2. Descriptions of the empirical technique are provided in Taha et al. (2008) and Rault (2005).

In an attempt to place the version 2.6 SL corrections on a more sound physical footing the version 2.5 empirical corrections were removed and replaced with PSF adjustments. We increased the tails of the PSFs for both UV and VIS/NIR by about 12% to account for the apparent underestimation of high altitude stray light photons. A contribution for in-band scattering by the primary telescope mirror has also been added to the PSFs. Telescope scattering was characterized during pre-launch testing but seems to have increased as a result of subsequent particulate contamination on the mirror surface. The pre-launch characterization was scaled by factors of 1.5 and 3 for the LP center and right (west) slits, respectively, at VIS/NIR wavelengths. The correction was not altered for the left slit or UV measurements from all three slits. Finally, a correction for out-of-band stray light originating longward of 1,000 nm was also introduced. Comparisons between measured and modeled radiances suggest that the changes were most effective at VIS wavelengths at tangent heights above 40 km.

The LP static radiometric calibration has been revised in the version 2.6 processing to use two-dimensionally (spectral x spatial) smoothed pre-launch albedo coefficients (radiance/irradiance). The “Day 1” calibrations are now based on solar measurements from orbit number 1864 on 7 March 2012. The “Day 1” wavelength scale assignment has also been updated based on measurements from this orbit. The solar irradiance measurements taken on “Day 1” are used to calculate sun-normalized radiances. This normalization is not updated over the mission lifetime though solar measurements occur every week. Instead, starting in version 2.6, solar measurements following “Day 1” are used to update Earth radiance calibrations. Corrections, derived by applying 5-pixel spectral smoothing of the solar data, do not exceed 3% for the mission lifetime at any wavelength (290–1,000 nm), nor at any spatial location. There is no indication these radiometric adjustments had a significant effect on the profile ozone time dependence because the adjusted calibration is mostly independent of altitude.

Version 2.6 utilizes these same weekly solar measurements to derive seasonal and long-term changes in wavelength registration. A seasonal spectral shift of amplitude 0.25 pixels was previously assigned to the data in a static pattern every year. A 1-pixel shift corresponds to approximately 0.75 nm band center shifts at 300 nm and 17 nm shifts at 1,000 nm due to the non-linear dispersion of the LP instrument. Dynamic use of the solar measurements now allows year-to-year variations in the seasonal pattern, and can account for long-term drifts in pixel band center wavelengths. The mean change in wavelength registration over the first 10 years of the SNPP mission is approximately 0.1 pixels. Changes in pixel band center wavelengths through each orbit, a result of thermally induced changes in spectrometer optics pointing, are registered the same as in previous versions (Jaross et al., 2014). As with the radiometric calibrations described in the preceding paragraph, spectral shifts are largely independent of altitude and thus have little effect on the altitude-normalized measurements used for ozone retrievals.

Accurate and stable altitude registration of limb scattering measurements is very important for retrieving high-quality ozone profiles suitable for climate studies, since an error of just 100 m in altitude can result in as much as a 3% error in ozone at altitudes above 35 km. The primary source of knowledge for the sensor pointing comes from the SNPP spacecraft attitude determination system consisting of two star-tracking devices. Despite that, a significant offset (∼1.4 km, adjusted in version 2) in the LP pointing was discovered shortly after launch, some of it apparently the result of a misalignment of the attitude control frame and the spacecraft body frame. The SNPP VIIRS instrument team also observed a shift. To complicate this matter, thermally induced distortions in the LP optics resulted in as much as a 1 km (depending on the slit) change in pointing from the ground to orbit. These same distortions result in measurable changes in wavelength and pointing during every orbit. Our baseline approach to LP altitude registration is to assume that the spacecraft attitude information is accurate but that additional adjustments are needed to account for distortions originating within OMPS. This assumption has one notable exception that we describe below.

Two scene-based methods have been developed (Moy et al., 2017) to assess altitude registration independent of the spacecraft attitude information. One method called Rayleigh scattering attitude sensing (RSAS), determines absolute altitude errors using a ratio of radiances at 350 nm between 20 and 30 km and external knowledge of the atmospheric pressure profile (Janz et al., 1996). The RSAS method is susceptible to inhomogeneity in the underlying Earth scene and aerosol interference, which limits its application to longer time scales and to regions and time periods with minimal aerosol contamination. Under these conditions it has an accuracy of ±200 m (Moy et al., 2017). The second method, called absolute radiance residual method (ARRM), looks at UV radiances shorter than ∼305 nm at altitudes between 60 and 65 km. These radiances have a sensitivity of 10%–15% per 1 km depending on the altitude and wavelength. The ARRM method is sensitive to errors in instrument absolute calibrations, and therefore it is used primarily to evaluate relative errors in altitude registration over short time periods. Its relative accuracy is also approximately ±200 m (Moy et al., 2017).

In the v2.5 processing we applied four types of altitude corrections: (a) static correction (1.37 km for the center slit); (b) 0.1 km jumps on 25 April 2013 to correct for a spacecraft attitude system calibration change and on 5 September 2014 to account for observed attitude changes; (c) intra-orbital adjustments of up to 0.3 km in the center slit to account for image motion at the focal plane; (d) additional, seasonally varying intra-orbital altitude corrections of ∼0.35 km for the center slit, with the greatest adjustments during June and July. The RSAS method was used to derive adjustments (a) and (b) while the ARRM method was used for adjustments (b) and (d). Adjustment (c) is derived by observing the locations of the entrance slit edges imaged on the oversized detector.

In version 2.6 we updated three of the four corrections: (a) static, (b) time-dependent, and (d) intra-orbital. For the center slit, the static correction now is 1.58 km (∼0.2 km change from version 2.5). The intra-orbital correction (d), still based on ARRM but simplified, now changes linearly as a fraction of orbit from south to north. The correction is the same for the three slits, and the seasonal dependence is removed. For the time-dependent correction (b), we left a single +0.1 km adjustment on 25 April 2013 to correct for the calibration adjustment that was acknowledged by spacecraft operators and confirmed by other instruments on the SNPP platform. The second 0.1 km step on 5 September 2014, implemented in version 2.5, was removed. All sensor pointing adjustments are applied to Level 1B measured radiances in version 2.6 processing.

After processing version 2.5 data, a 0.1-km drift was detected by the RSAS method in sensor pointing (Kramarova et al., 2018). The comparisons between LP version 2.5 and MLS ozone revealed a positive drift of ∼0.5%/yr that was more pronounced at altitudes above 35 km with the pattern consistent with a possible drift in sensor pointing

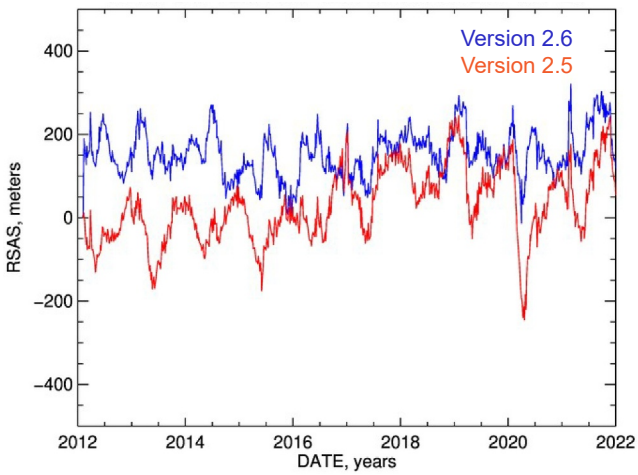

Figure 1. RSAS (Rayleigh Scattering Attitude Sensing) time series for versions 2.5 (red) and 2.6 (blue) from April 2012 through December 2021 in the Southern Hemisphere (50°S–20°S). The results are illustrated as errors in the instrument pointing expressed in meters. The RSAS method is sensitive to aerosol interference, therefore we limited the region to the southern mid-latitudes where the LP measurement sensitivity to aerosol as well as aerosol contamination are minimum. The Hunga eruption in January 2022 injected large amounts of aerosol into the stratosphere and as a result substantially affected the RSAS record (see Section 2.2.5 and Figure S9 in Supporting Information S1).

(Kramarova et al., 2018). The drift in version 2.5 ozone was also reported in other independent studies (e.g., Wargan et al., 2020) and in other independently processed OMPS-LP products (e.g., Arosio et al., 2024). We believe the September 2014 adjustment contributed to this apparent drift.

Figure 1 shows the RSAS time series for the center slit. The 0.2 km offset between the two versions is clearly seen at the beginning of the record. Though the figure suggests the version 2.6 static adjustment has driven RSAS results further from zero, the observed offset is within the uncertainty of the technique. The version 2.6 RSAS time series has smaller interannual variability due to updated aerosol corrections and simplified seasonal pointing correction. The version 2.5 RSAS has a clear upward drift by about +0.15 km over 10 years, which is not present in version 2.6. The step in September 2014, now seen in version 2.6 RSAS, is no different than similar steps such as in March 2019. There is no justification to suspect that these periodic steps affect the long-term accuracy of the spacecraft attitude knowledge. The lack of any significant RSAS drift in the version 2.6 data leads us to conclude we may continue relying on the spacecraft attitude information to derive the LP altitude registration.

2.2.2. Version 2.6 LP Ozone Retrieval Algorithm

In version 2.6, we updated ozone and NO_2 absorption cross-sections and climatologies. In the UV spectral range (295–355 nm), Brion-Dumont-Mallicet (BDM) (Brion et al., 1993) cross sections provide more accurate ozone absorption coefficients at longer UV channels ($\lambda > 320$ nm) compared to Bass and Paur (1985) cross-sections we used previously. BDM cross-sections are also used by the ozone retrieval algorithms that derive ozone columns and profiles from the SNPP OMPS nadir instruments (NM and NP). In the VIS range, Serdyuchenko-Gorshelev (SG) cross-sections (Gorshelev et al., 2014) replaced those by Burkholder and Talukdar (1994). Nitrogen dioxide (NO_2) cross-sections from Mérienne et al. (1995) were replaced with those from Vandaele et al. (1998) in version 2.6.

The retrieval algorithm needs ozone a priori profiles, and we use an updated seasonal ozone climatology (Ziemke et al., 2021) in version 2.6 that is based on multi-year averaged MLS ozone profiles in the stratosphere and model simulations with the Goddard Earth Observing System (GEOS) Global Modeling Initiative (GMI) model in the troposphere. Previously, we used McPeters and Labow (2012) climatology based on a set of MLS and sonde measurements. The NO_2 climatology was constructed using the GEOS GMI model (Fisher et al., 2024). Since stratospheric NO_2 concentration varies significantly during the day, the NO_2 climatology has an additional dimension of local solar time (90 bins), in addition to 36 5-degree latitude bins and 12 seasonal bins. We discuss sensitivity of the LP ozone algorithm to changes in these parameters in Section 2.2.4.

Aerosol attenuation affects ozone retrievals; therefore, we explicitly correct for this effect using aerosol extinction profiles retrieved concurrently from the same OMPS LP measurements at 675 nm. To retrieve aerosol extinction profiles (Loughman et al., 2018) we need to assume an aerosol particle size distribution. In version 2.6, we use the gamma-function particle size distribution, which replaces the bimodal function used in version 2.5. Chen et al. (2018) has shown improvements in retrieved aerosol at 675 nm after switching to the gamma-function distribution. The radiance adjustment at ozone sensitive wavelengths is computed using the same gamma-function particle size distribution.

Any clouds located along the LP line of sight shield the radiances scattered from lower altitudes and reflect a large portion of the incoming radiation. The LP cloud detection algorithm (Chen et al., 2016) uses the spectral dependence of the vertical gradient in radiance between two wavelengths in the visible and near-IR spectral bands (674 and 868 nm) to discriminate between clouds and aerosols. Once a cloud is identified we start ozone profile retrievals at an altitude 1 km above the cloud top height.

To simulate limb-scattered radiances in the forward model we use the Gauss-Seidel Limb Scattering (GSLS) radiative transfer model (Herman et al., 1994; Loughman et al., 2005, 2015). Before simulating radiances, we first

10.1029/2024EA003707

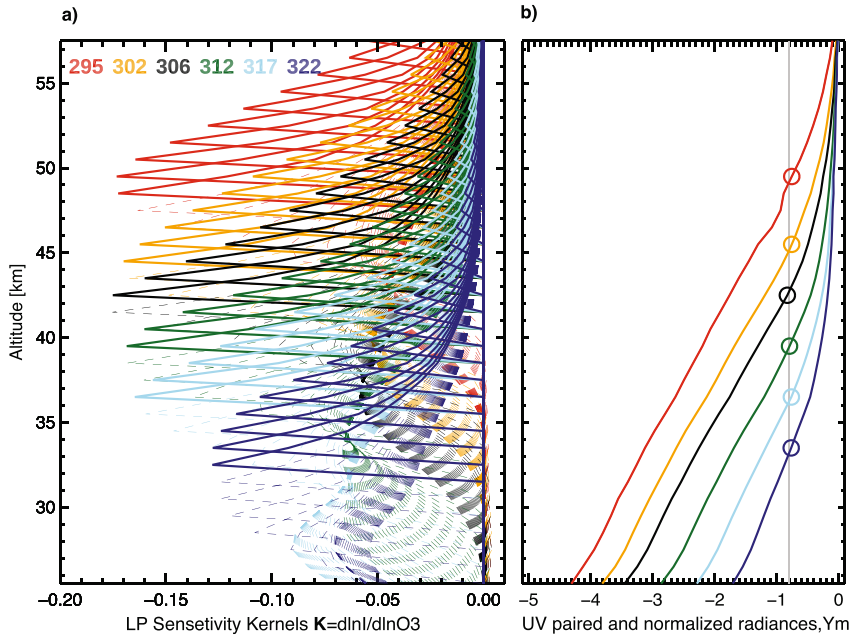

Figure 2. Left panel shows LP sensitivity kernels dY(z,λ)/dln(O3) for 6 UV pairs. Right panel shows vertical profiles of measured radiances normalized at 60.5 km and paired with the reference 353 nm wavelength. Colors represent different UV pairs. The vertical gray line indicates $Y = -0.8$—the threshold used to cut UV pairs in the LP algorithm. Color circles show the lowest altitude where the given pair is used by the algorithm. Dashed lines on the left panel show that kernels below the lowest altitude used for each pair have decreasing magnitudes.

derive the scene reflectivity from the LP measurements at 675 nm. If a cloud is detected, an effective surface reflectivity is computed to represent a weighted average of the surface and cloud reflection, considering any clouds as being present at the terrain height (Lambertian effective reflectivity approach).

In the ozone retrieval algorithm we use sun-normalized radiances, that is, scattered radiances normalized by their solar irradiance counterparts, to reduce the influence of spectral and irradiance calibration errors (Jaross et al., 2014). To further minimize the sensitivity of the ozone retrieval to absolute instrument calibration as well as to reduce effects of the underlying scene reflectivity and errors in the forward model, measured radiances are normalized with radiances measured at high altitudes where sensitivity to ozone for a given wavelength is negligibly small (Flittner et al., 2000). In the version 2.6 algorithm, UV radiances are normalized at 60.5 km and VIS radiances at 40.5 km. Ozone climatological profiles (Ziemke et al., 2021) are used to simulate radiances at and above the normalization altitude. Climatological profiles are scaled at each iteration based on retrieved ozone values from the previous iteration at altitudes 5 km below the normalization altitude.

A key difference between this release and previous versions is that a single merged ozone profile is retrieved using UV and VIS measurements between 12.5 km (or cloud top) and 57.5 km. Ozone profiles in previous versions were retrieved independently from UV and VIS measurements using wavelength pairs in the UV range and triplets in VIS (e.g., Kramarova et al., 2018; Rault & Loughman, 2013). The version 2.6 algorithm uses radiances measured at six UV ozone-sensitive wavelengths (295, 302, 306, 312, 317, and 322 nm) paired with 353 nm and one VIS wavelength at 606 nm combined with 510 and 675 nm to form a triplet. The approach when ozone-sensitive wavelengths are combined with the reference wavelength(s), which have almost no ozone absorption, to form a pair or a triplet, minimizes the algorithm's sensitivity to the atmospheric pressure and temperature profiles used in the forward model calculations to simulate radiances (Flittner et al., 2000). Wavelength pairs and triplets also help to reduce the sensitivity of the retrieval algorithm to aerosols.

Each wavelength pair is used over a limited range of tangent point altitudes determined from the vertical shape of sensitivity kernels and measured radiances (see Figure 2). Limb scattered radiances at ozone sensitive wavelengths first increase as they propagate to lower altitudes and then reach the knee—a saturation when the radiances are no longer changing with altitude anymore (e.g., Degenstein et al., 2009). Below the knee altitude, the

UV channel become insensitive to changes in ozone which is also reflected in the decrease of the sensitivity kernels **K** (Figure 2a). We found that the tangent altitude z where the sensitivity kernels **K** start to degrade (Figure 2a) corresponds to the altitude where paired and altitude normalized radiances Y_m get smaller than −0.8 (Figure 2b). The vertical range for each pair is dynamic and changes from one profile to the next, but for the same UV pair the range varies within 2–4 km (see Table S1 in Supporting Information S1). We selected UV pairs to maintain a near-constant sensitivity of the algorithm to changes in ozone over the entire vertical range from 12.5 to 57.5 km.

The version 2.6 algorithm uses the optimal estimation framework (Rault & Loughman, 2013; Rodgers, 2000) to iteratively retrieve ozone profiles $\boldsymbol{X}$:

$$\boldsymbol{X}_{i+1} = \boldsymbol{X}_i + \left(\mathbf{S_a^{-1}} + \mathbf{R^T R} + \mathbf{K^T S_\epsilon^{-1} K}\right)^{-1}\left[\left(\mathbf{S_a^{-1}} + \mathbf{R^T R}\right)(\boldsymbol{X}_a - \boldsymbol{X}_i) + \mathbf{K^T S_\epsilon^{-1}}(\boldsymbol{Y} - \boldsymbol{F}(\boldsymbol{X}_i))\right] \quad (1)$$

Where i is the index that indicates the ith iteration, $\boldsymbol{X_a}$—a priori climatological ozone profile, $\mathbf{S_a}$—a priori covariance matrix constructed as a diagonal matrix with the diagonal elements equal to the square of the a priori ozone values at that altitude $S_a(k, k) = X_a{}^2(k)$; $\mathbf{S_\epsilon}$− measurement noise covariance matrix is a diagonal matrix with the prescribed 1% noise for UV pairs. For the VIS triplet, noise is 0.5% for 27.5 km and below and gradually increases above 27.5 km reaching 1% at 37.5 km. The measurement vector $\boldsymbol{Y}$ consists of 6 UV pairs and one VIS triplet. The GSLS radiative transfer model is employed to simulate radiances $\boldsymbol{F}(\boldsymbol{X_i})$ using a retrieved ozone profile from a previous iteration (or ozone climatological profile $\boldsymbol{X_a}$). $\mathbf{K} = \partial \mathrm{Y}/\partial \mathrm{X}$ is a matrix of weighting kernels (or Jacobian), each element of which represents the partial derivative of measurement vector $\boldsymbol{Y}$ to a state vector $\boldsymbol{X}$ (see also Figure S1 in Supporting Information S1). The weighting kernels **K** are calculated by the GSLS forward model and updated after each iteration. In version 2.6, we use the second order Tikhanov's regularization (term **R,** Livesey et al., 2006; Rault & Loughman, 2013) to improve stability of the ozone retrievals and to obtain a vertical resolution of ∼2.0 km for ozone retrievals $\boldsymbol{X}$ across all altitudes. The vertical resolution of LP ozone profiles is ∼1.9–2.5 km between 20 and 55 km, degrading to ∼3–8 km at lower and higher altitudes. We use the Levenberg-Marquardt method to solve Equation 1 which helps finding the solution for the non-linear problem by reducing the step between iterations. The LP daily files include only a limited number of algorithmic parameters, but many parameters required (von Clarmann et al., 2020) for the error analysis are included in the Level 2 orbital files, which can be provided upon request.

2.2.3. Quality Flags in Version 2.6 Processing

The accuracy of LP retrieved ozone profiles depends on the combination of many individual factors. We report a set of quality flags to data users for filtering OMPS LP ozone retrievals. The algorithm runs a convergence test to determine when the iterations can be stopped using the following equation (Rodgers, 2000):

$$d_i^2 = (\boldsymbol{X}_i - \boldsymbol{X}_{i-1})^T \hat{\mathbf{S}}^{-1} (\boldsymbol{X}_i - \boldsymbol{X}_{i-1}) \quad (2)$$

where $d^2{}_i$ is a convergence criterion after the ith iteration and $\hat{\mathbf{S}}$ is the solution covariance matrix defined as:

$$\hat{\mathbf{S}} = \left(\mathbf{S_a^{-1}} + \mathbf{R^T R} + \mathbf{K^T S_\epsilon^{-1} K}\right)^{-1} \quad (3)$$

The iterations are stopped when the convergence criterion reduces with iteration ($d^2{}_i < d^2{}_{i-1}$) and gets smaller than 10 ($d^2{}_i < 10$). If after seven iterations these conditions are not met, we assume that the retrieval did not converge and was not successful. Fewer than 1% of profiles have convergence values $d^2 > 10$ after seven iterations. Typical number of iterations varies between 2 and 7. Users are thus recommended to use only profiles with the number of iterations (variable O3Status) ranging from 2 to 7 (inclusive) and the convergence less than 10 (variable O3Convergence).

The estimated precision for each profile retrieval is calculated using the square roots of diagonal elements of the solution covariance matrix $\hat{\mathbf{S}}$ (from Equation 3 above). Precision values range between 3% and 4% at altitudes between 20 and 52 km (Figure 3). Larger precision values occur in the tropical upper troposphere and lower stratosphere (UT/LS) and in the mesosphere above 50 km.

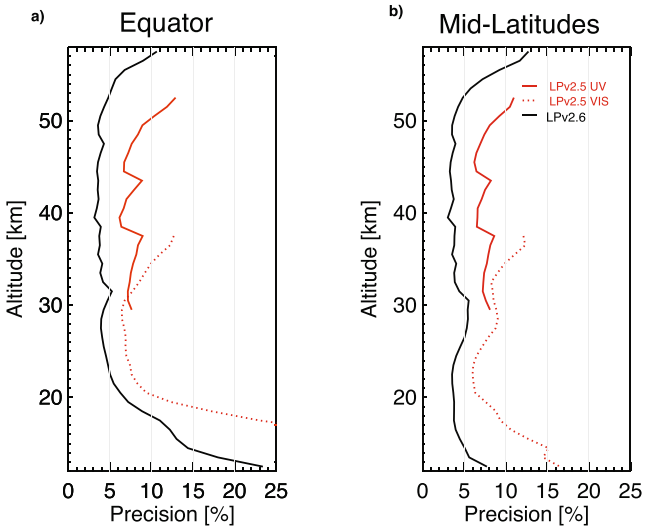

Figure 3. Retrieval precision of OMPS LP ozone profiles in % for version 2.5 (red lines) and version 2.6 (black line) in the tropics (a) and mid-latitudes (b) on 1 March 2015, orbit 17,307, events 110 [15.9°N, 110.6°E] and 136 [44.2°N, 102.6°E], respectively. In version 2.5 precision was systematically larger indicating lower confidence.

The LP algorithm uses a predefined set of wavelengths. Occasionally, measurements at the required wavelengths are not available and the algorithm looks for the nearest available wavelength within ±0.4 nm in the UV region and ±2.0 nm in VIS from the nominal wavelength. The retrieved profile will be flagged (ozone quality flag) if the algorithm cannot find measurements within the defined range. Users are recommended to use only profiles with the quality flag set to zero (i.e., O3quality = 0). Approximately 1% of retrieved profiles are flagged in this manner.

Polar Mesospheric Clouds (PMCs) form at altitudes of around 80–85 km over polar latitudes (>50°) in the summer months. PMCs can affect limb measured radiances at tangent altitudes as low as 50 km if the clouds are in the line of sight (LOS) of the LP instrument. PMCs increase scattering, and the magnitude of the excess signal produced by PMCs is greater in the NH because PMC particles have an increased phase function in forward-scattering geometry (DeLand & Gorkavyi, 2020). This excessive scattering by PMCs can lead to an underestimation of ozone concentration, which we typically see in the upper portion of ozone profiles (above 35 km). We identify PMC events by analyzing limb radiances at altitudes above 60 km and flag them in the output files. This flag more often occurs in the Northern Hemisphere (see Figure 4a). We recommend users to not use profiles affected by PMCs (i.e., only use profiles with ASI_PMC flag = 0). The PMC flag eliminates about 4%–4.5% of data during summer months in both hemispheres (see also Figure S2 in Supporting Information S1).

The retrieval algorithm aims to minimize the differences between measured and simulated radiances. After the algorithm converges, we simulate radiances again using the retrieved ozone profile. If the differences between simulated and measured radiances are still larger than the assumed measurement noise (Kramarova & DeLand, 2023), we flag those retrievals using the quality measurement vector (QMV) flag. The QMV flag eliminates about 2%–2.5% profiles, including cases when the measurements are affected by charged particles. We therefore recommend removing any profile where the QMV flag is not equal to zero. Contamination of LP radiance measurements by charged particles happens regularly when the satellite flies over the South Atlantic Anomaly (SAA) region (see Figure 4b), but occasionally, it also happens outside that region. Any pixel on the LP CCD detector can be affected by charged particles, meaning that measurements at any wavelength and at any tangent altitude can be compromised. The frequency of the QMV flag does not vary seasonally or over the time of the SNPP mission (see also Figures S3 and S4 in Supporting Information S1), which is consistent with the majority of radiance anomalies having resulted from SAA transients.

For scientific applications, we highly recommend using all these flags to filter out ozone retrievals with lower quality. Accept profiles with the following parameters:

- The convergence criterion d^2 less than 10 (O3Convergence < 10);
- The number of iterations ranging between 2 and 7 inclusively (2 ≤ O3Status ≤ 7);
- No PMC contamination (ASI_PMCflag = 0);
- Final residuals are smaller than assumed measurement noise (QMV = 0);
- Measurements at all required wavelengths are available (O3Quality = 0).

2.2.4. Analysis of Algorithmic Characteristics

In this section we discuss the version 2.6 algorithm performance. Averaging kernels are important components of the retrieval algorithm that characterize its sensitivity to true ozone changes. Version 2.6 averaging kernels are more consistent throughout the entire stratosphere (see Figures 5c and 5d), while version 2.5 kernels (Figures 5a and 5b) sharply decrease at altitudes where the algorithm switches wavelengths. The combination of additional wavelengths and regularization applied in the version 2.6 algorithm improved consistency of the averaging kernels in terms of peak magnitude and width. The version 2.6 algorithm is able to maintain a uniform sensitivity throughout the entire vertical range. Using averaging kernels, we estimate that the degrees of freedom for the signal in version 2.6 is around 18–20. The vertical resolution of retrieved ozone profiles can also be estimated as

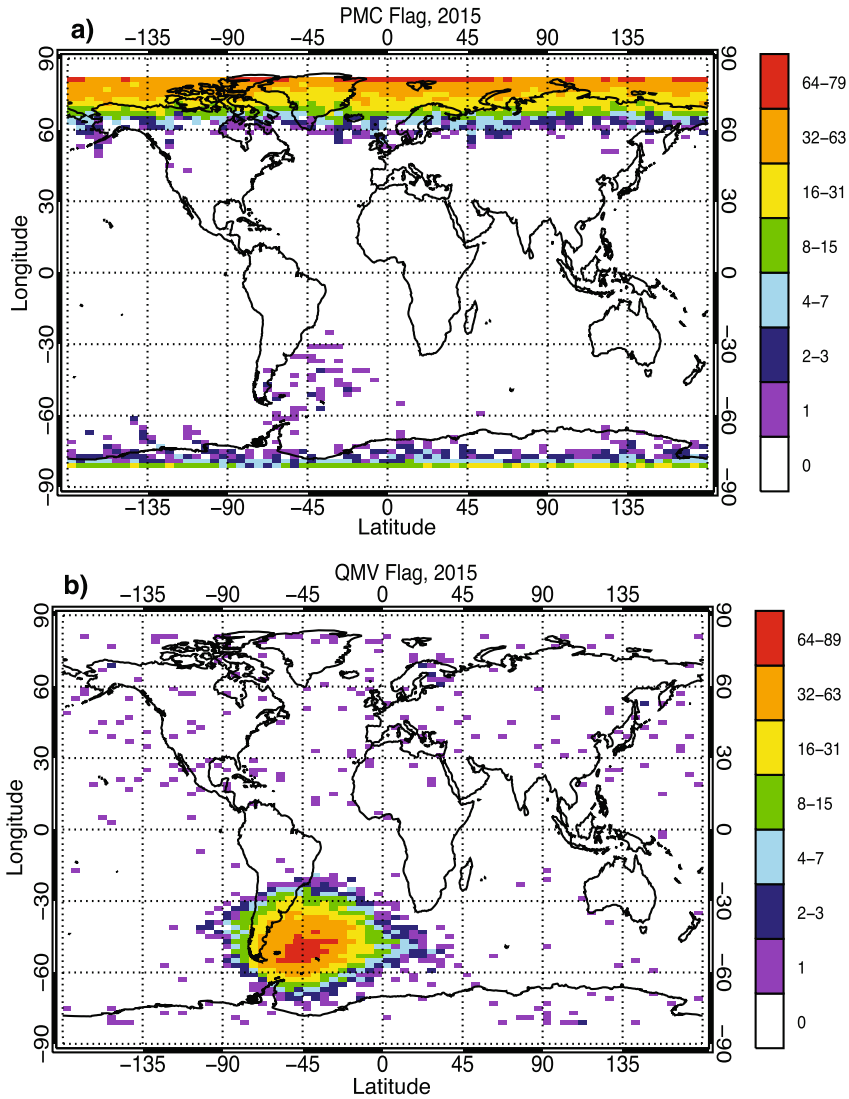

Figure 4. Spatial distribution of the PMC (a) and QMV (b) flags in 2015. The data are shown for 5° by 2° spatial bins (longitude°×°latitudes) and expressed as the total number of profiles illuminated by the PMC (a) or QMV (b) flag in 2015. Increased flagging occurs south of the geographic location of the SAA because the tangent points are 3,000 km distant from the satellite itself.

the inverse of the diagonal elements of the averaging kernel matrix (Rodgers, 2000). The vertical resolution (Figure 5 and also Figure S5 in Supporting Information S1) in version 2.6 ranges between 1.9 and 2.5 km, and is slightly degraded compared to the 1.7–2.0 km vertical resolution in version 2.5 (Kramarova et al., 2018). In the tropics the algorithm sensitivity below the ozone peak (below ∼20 km) drops sharply (Figures 5a and 5c) leading to the vertical resolution of only 4–10 km in the lowermost tropical stratosphere and upper troposphere (12–20 km) for cloud-free scenes.

The algorithm sensitivity to the a priori can be also estimated using the averaging kernels (Rodgers, 2000). The LP ozone retrieval algorithm is very insensitive to a priori (see Figure S6 in Supporting Information S1) between 17 and 52 km in mid-latitudes and about 22–52 km in the tropics (Arosio et al., 2022). Sensitivity to a priori increases at the upper (above 52 km) and lower portion (below 17 km in mid-latitudes and 22 km in the tropics) of the profile where sensitivity of the LP measurements to ozone sharply declines.

To estimate the algorithm sensitivity to changes in algorithmic parameters, such as the replacement of ozone and nitrogen dioxide absorption coefficients, updates in ozone and nitrogen dioxide climatologies, and changes in

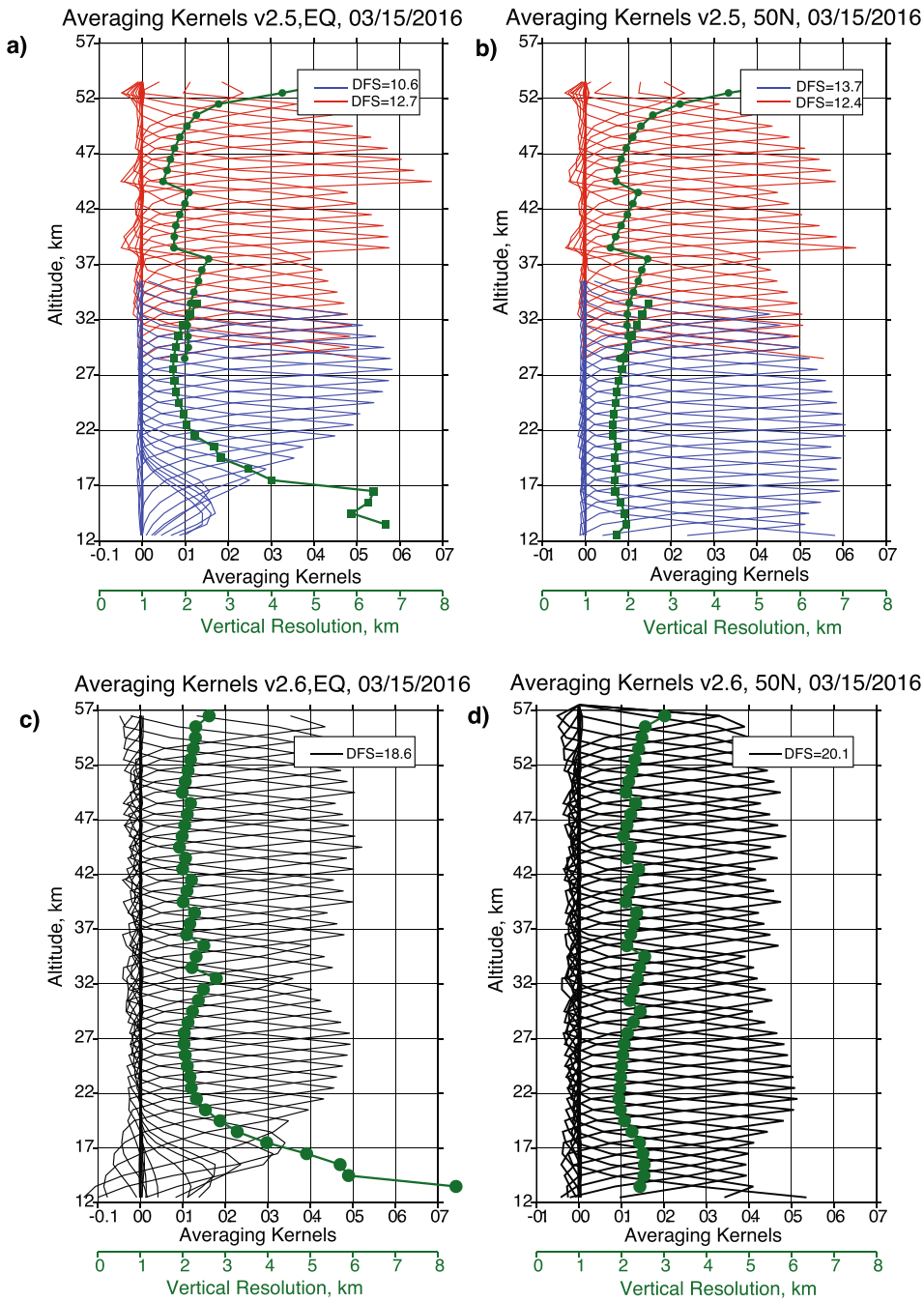

Figure 5. Typical LP averaging kernels and vertical resolution in the tropics (a and c) and in mid-latitudes (b and d). Panels (a) and (b) show version 2.5 kernels for UV (red) and VIS (blue) retrievals, and the vertical resolution is shown in green with additional *X*-axis scale. Total degrees of freedom for the signal, calculated as the sum of diagonal elements, are shown on the labels. Panels (c) and (d) show kernels and vertical resolution for the same events from version 2.6 (15 March 2016, orbit 22,696, events 91 and 136, respectively).

aerosol particle size distribution, we ran a series of tests in which we replaced one parameter at a time and retrieved ozone for a day. We calculated responses in ozone retrievals as differences between standard version 2.6 and the test with the perturbed parameters. It is important to note that the aim of these tests was not to explain differences between versions 2.5 and 2.6, but rather to evaluate sensitivity of the version 2.6 algorithm to changes in these parameters. We found that replacement of nitrogen dioxide (NO_2) cross sections from Mérienne et al. (1995) to Vandaele et al. (1998) resulted in about 0.5%–1% decrease in retrieved ozone in the altitude range

between ~32 and 36 km. This is due to increasing NO_2 absorption at longer UV wavelengths (322 nm pair), which are used by the LP algorithm in this altitude range, and increasing NO_2 concentration which peaks around 30 km (see Figure S7 in Supporting Information S1). In the second test, we estimated how the replacement of the NO_2 climatology from the PRATMO (PRather ATmospheric Model) photochemical box model (Brohede et al., 2007; Prather & Jaffe, 1990) to GEOS GMI (Nielsen et al., 2017; Orbe et al., 2017) affected retrieved ozone. This switch in NO_2 climatology produced almost no change in retrieved ozone above 30 km (<0.2%), but produced a small negative bias of ~−0.5% below 30 km, particularly in mid-latitudes in both hemispheres (see Figure S7 in Supporting Information S1).

The replacement of ozone cross-sections from Bass and Paur (1985) in the UV and Burkholder and Talukdar (1994) in the VIS to Brion-Dumont-Mallicet (BDM) (Brion et al., 1993) and Serdyuchenko-Gorshelev (SG) (e.g., Gorshelev et al., 2014), respectively, produced systematic differences in ozone retrievals, particularly above 30 km. Retrievals that use BDM cross-sections yielded 1%–2% larger ozone concentrations between 30 and 48 km, and reduced ozone above 50 km by ~−0.5%. Below 30 km ozone slightly increased by ~0.5–0.8% (see Figure S7 in Supporting Information S1).

The switch in ozone climatology used as a priori produced almost no changes in retrieved ozone profiles between 22 and 52 km in the tropics and between 17 and 52 km outside the tropics. This is because the LP algorithm is not sensitive to a priori. However, we found small oscillations of ±0.2–2% in the ozone differences when we changed ozone climatologies, but these oscillations have a narrow 1-km width (see Figure S7 in Supporting Information S1). The retrieval algorithm behaves as a low-frequency filter, and any fine scale structures either in the measurements or a priori that are finer than the vertical resolution can not be retrieved. Therefore, it is very important to have smooth a priori profiles without any sharp vertical gradients. We found that the ozone climatology used in version 2.5 had sharp vertical gradients and was responsible for vertical oscillations in the test results (see Figure S8 in Supporting Information S1). Overall, updates in these four algorithmic parameters produced very small (less than ±1–2%) but systematic changes in ozone retrievals.

We observed much larger changes in ozone retrievals (Figure 6) after switching the assumed aerosol particle size distribution from bimodal (Loughman et al., 2018) to gamma-function (Chen et al., 2018). The ozone retrievals are corrected for aerosols using the aerosol extinction coefficient profile derived from concurrent aerosol observations at 675 nm retrieved from the same LP measurements. The radiance adjustment at ozone sensitive wavelengths is computed using the assumed particle size distribution. The largest negative changes in ozone retrievals occur in the tropical lower stratosphere and upper troposphere (below ~22 km), where changes can reach up to 35% in the 12.5–15.5 km range (Figure 6). The sensitivity of the LP measurements to aerosols is very weak in the Southern Hemisphere, due to the aerosol phase function being much smaller in the back-scattering direction that LP measures. Therefore, changes are very small in the southern mid- and high latitudes (less than ±1%). In the northern subtropics, mid- and high-latitudes, sensitivity to aerosol is much stronger, resulting in larger differences in the retrieved ozone due to the change in assumed aerosol particle size distribution (Figure 6). We see negative changes (up to −5%) in the northern subtropics and mid-latitudes (EQ55°N) between 20 and 32 km, and positive changes (up to 3%–8%) at high latitudes (60°N–82°N). The changes are very small above 32 km where the algorithm uses UV measurements, and the concentrations of background stratospheric aerosols are typically very low.

2.2.5. Effect of the Hunga Volcanic Aerosols on LP Ozone Retrievals

The explosive eruption of the Hunga volcano on 15 January 2022 injected aerosols and water vapor into the stratosphere and substantially increased stratospheric aerosol optical depth (Taha et al., 2022). Volcanic material was detected at altitudes as high as 58 km shortly after the eruption which had never been observed during the satellite era. For several months immediately after the eruption, the aerosol concentration was very high, exceeding 1.5×10^{-3} km^{-1} at altitudes up to 27 km near the ozone density peak (Figure 7a). The total optical depth at 675 nm, integrated along the line of sight, was greater than 8 for one orbit the day after the eruption (Figure 7b). The volcanic aerosol increased scattering, leading to sharp increases in LP radiances. The increased aerosol burden compromised the RSAS technique which we use to monitor the instrument pointing (Figure S9 in Supporting Information S1). For several months, the LOS optical depth was greater than 1 at tangent altitudes near the ozone peak (23–26 km), making ozone retrievals impossible below 20–25 km. To eliminate profiles affected by volcanic aerosol we use retrieved aerosol extinction profiles at 675 nm. If the retrieved extinction at 675 nm is

10.1029/2024EA003707

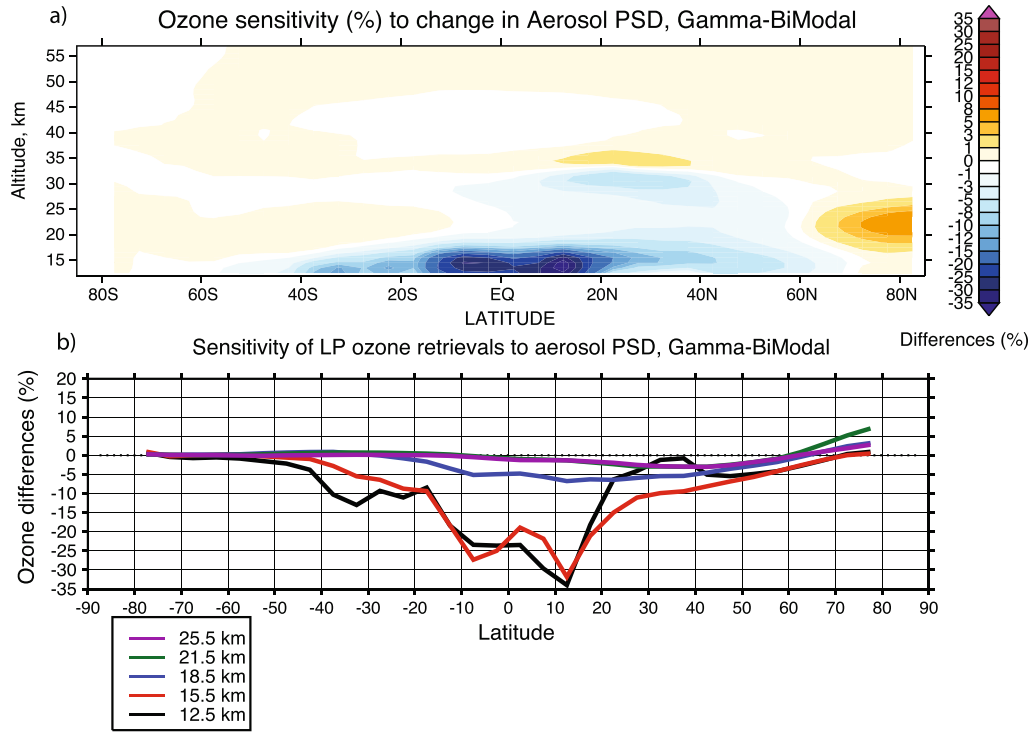

Figure 6. Sensitivity of the LP algorithm to a change in the aerosol particle size distribution from bimodal to gamma-function, which is equivalent to the change in aerosol models between versions 2.5 and 2.6. The upper panel (a) shows daily zonal mean differences in percent (note that the color scale is non-linear) as a function of latitude and altitude. The lower panel (b) shows daily zonal mean differences as a function of latitude for five levels in the lower stratosphere between 12.5 and 25.5 km.

greater than 1.5×10^{-3} km^{-1} at any altitude above 18.5 km, we cut ozone retrievals at and below that altitude (retrieved ozone values are set to a fill value). As a result of this filtering, there are gaps in the LP ozone record in the lower stratosphere (below 25 km) mostly in the tropics and SH mid-latitudes, for 12–18 months after the eruption (see Figure S10 in Supporting Information S1).

As seen in Figure 7a, the volcanic aerosol slowly descended in the second half of 2022 (e.g., Schoeberl et al., 2023; Taha et al., 2022) and spread into mid- and high- latitudes in both hemispheres. As the aerosol optical depth declines, the number of successful ozone retrievals in the lower stratosphere increases.

3. Evaluation of OMPS LP Ozone Profiles

Ozone profile retrievals from OMPS LP were evaluated previously (Kramarova et al., 2018) by comparing with independent satellite profile measurements obtained from the Aura Microwave Limb Sounder (MLS), Atmospheric Chemistry Experiment Fourier Transform Spectrometer (ACE-FTS) and Odin Optical Spectrograph and InfraRed Imaging System (OSIRIS). The study found that the mean differences between LP version 2.5 and correlative measurements are well within ±10% between 18 and 42 km meeting the instrument requirements (Flynn et al., 2006) and in many places are within ±5%. A positive drift of ~0.5%/yr was detected in the LP ozone record against MLS and OSIRIS with the pattern consistent with a possible 100 m drift in the LP sensor pointing.

In this paper we evaluate the version 2.6 ozone profile data set over 10+ years and we limit our evaluation to comparisons with Aura MLS. The goal is to document mean differences and long-term drifts between the two OMPS LP versions (version 2.5 and 2.6) using MLS as a reference. A complementary study will follow, and it will provide a comprehensive evaluation of version 2.6 against a larger set of correlative satellite and ground-based observations.

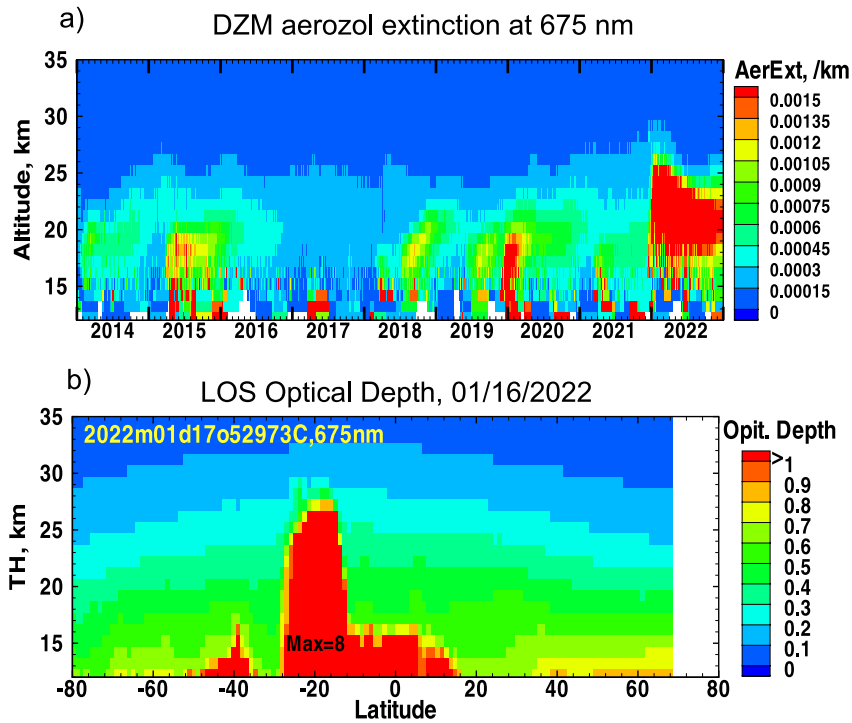

Figure 7. Upper panel shows daily zonal mean values of aerosol extinction in SH subtropics (15°–20°S) over the SNPP mission. Typical background aerosol extinction is $<<10^{-3}$ km^{-1}, particularly above 15 km, but extinction increases after volcanic eruptions (e.g., Calbuco eruption in 2015) or mega wildfires (2019–2020 New Year Australian fires). The Hunga eruption injected aerosol to an unprecedented height and increased zonally averaged aerosol extinction in the stratosphere to levels $>1.5 \times 10^{-3}$ km^{-1}. Lower panel shows LOS optical depth at 675 nm for one orbit (52,958) on 16 January 2022. The LOS optical depth was well above 1 in the region near the eruption (with the maximum estimated LOS depth ~8). Ozone retrievals are not possible in conditions when the LOS optical depth exceeds 1.

3.1. Correlative Measurements

The Aura MLS record started in August 2004, and overlaps for more than 12 years with SNPP OMPS LP. The equatorial crossing time of SNPP and Aura are very similar, and on some days (about once a month) the two orbits are perfectly co-located. The vertical resolution of the MLS ozone retrievals in the stratosphere is 3 km and decreases to 5.5 km in the mesosphere. We use the latest version 5 of MLS data (Livesey et al., 2022). For validation with the limb scattering OMPS LP, we limited MLS data to daytime observations (solar zenith angle <89°); and we filtered MLS data using criteria recommended by the MLS Team.

3.2. Comparison Technique

In this study, for comparisons between OMPS LP and MLS, our spatial and temporal collocation criteria are the following: profiles should be within ±2° latitude from each other with the distance between them less than 1,000 km and the time difference within ±5 hr. We analyze ozone profiles on the LP native coordinate system (number density on altitude grid), which requires unit conversion for MLS retrievals. MLS volume mixing ratio profiles were first interpolated on the LP regular altitude scale using GEOS FPIT (Lucchesi, 2013) pressure profiles reported with OMPS LP data. Then, these interpolated mixing ratio profiles were converted into number densities using the GEOS FPIT ancillary pressure and temperature profiles. Since the LP algorithm does not retrieve ozone below the cloud top, we cut matching MLS ozone profiles at the cloud top altitude as well to avoid biases due to different sampling in cloudy and cloud-free conditions. In this study, we do not account for small differences in the vertical resolution of the instruments. We further binned matched LP and MLS profiles into 5-degree latitude bins. We adopted the same methodology described in Kramarova et al. (2018) to calculate biases and drifts.

10.1029/2024EA003707

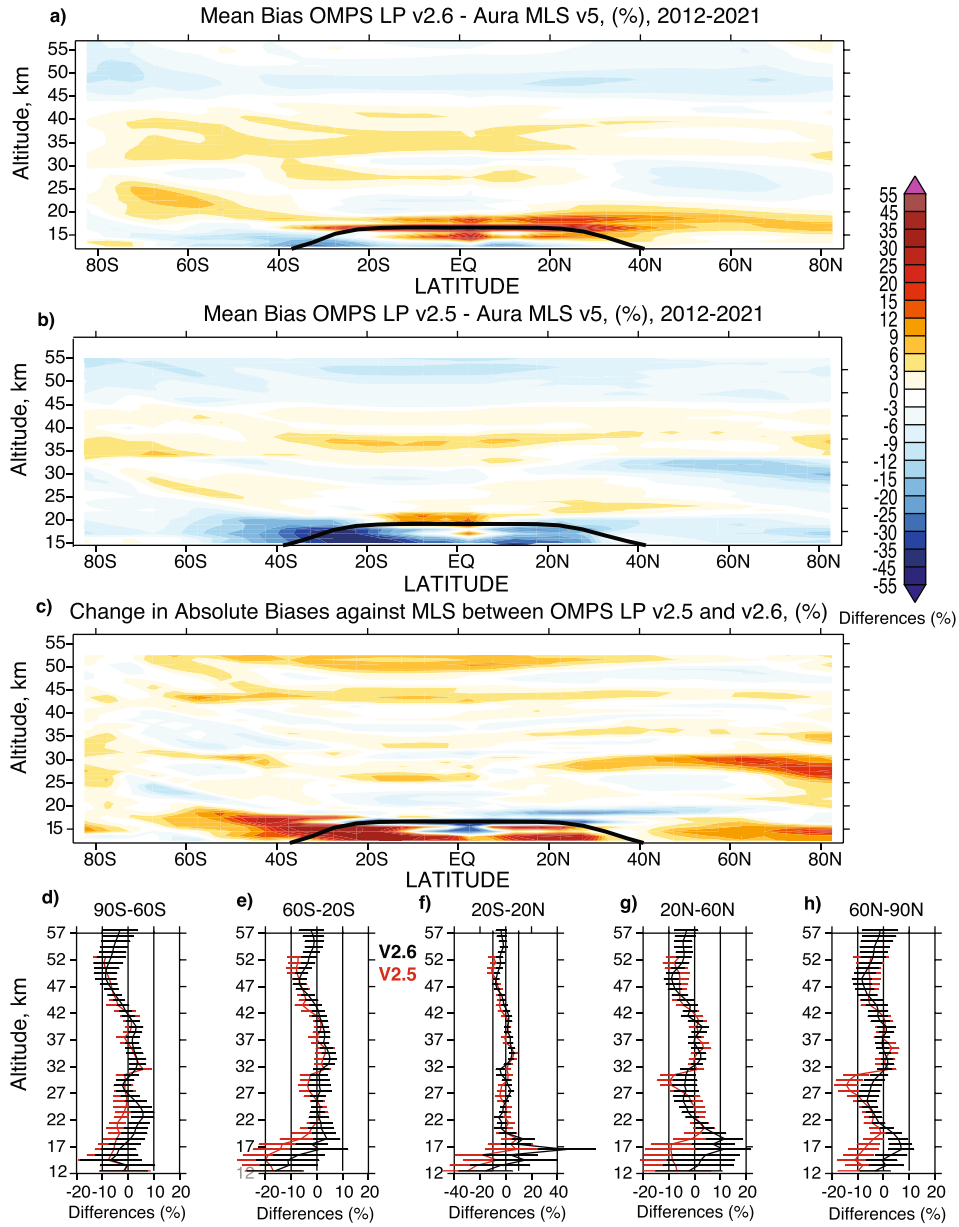

Figure 8. Mean biases between OMPS LP and MLS version 5 over 10 years between April 2012–December 2021. Panel (a) shows mean biases in percent (%) for version 2.6 of OMPS LP data as a function of altitude between 12.5 and 57.5 km and latitude (5-degree grid). The black solid line shows the mean tropopause height. Panel (b) is the same as panel (a) but for version 2.5. Panel (c) shows changes (%) in absolute biases against MLS between versions 2.5 and 2.6, essentially differences between absolute values shown in panels (b) and (a). Panels (d–h) show biases between versions 2.6 (black lines) and 2.5 (red lines) against MLS in 5 wide latitude bins. Horizontal lines represent 1 standard deviation for mean differences. The standard error of the mean is typically smaller than the width of the lines.

3.3. Results and Discussions

Since version 2.5 data had not been screened for the Hunga anomalies, we limit the time period for comparisons to April 2012 through December 2021. In version 2.5, UV and VIS retrievals are done independently, so we use VIS retrievals between 12.5 and 30.5 km and UV retrievals above 30.5 km.

The differences between the two LP versions are not large in the upper part of the profiles above ~32 km (see Figure 8). The biases between LP version 2.6 and MLS are mostly within ±5% between 20.5 and 45.5 km. Both

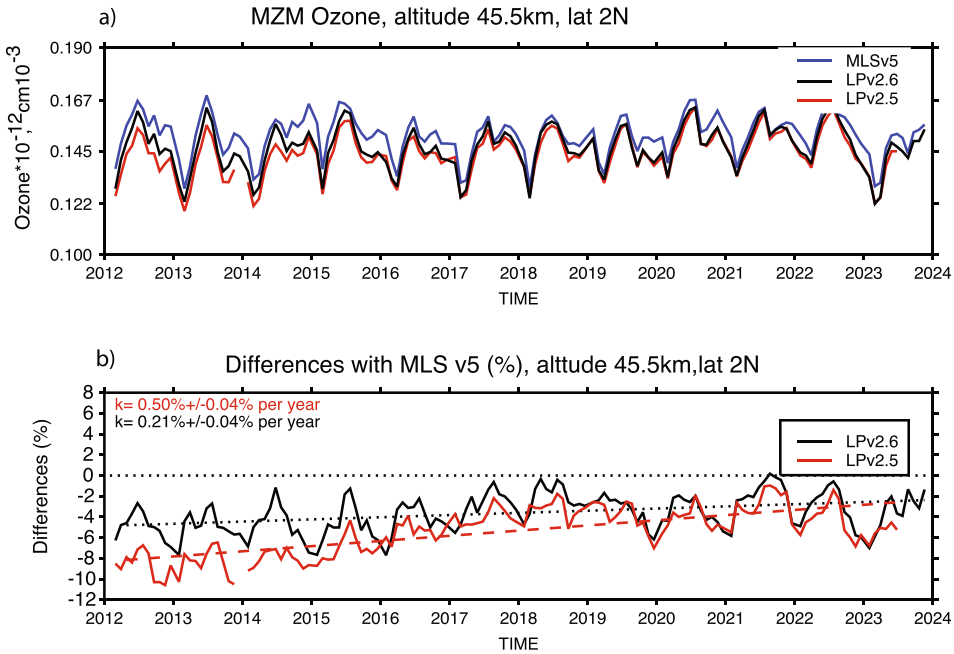

Figure 9. (panel a): LP and MLS time series of ozone number density at 45.5 km, where LP retrievals are most sensitive to the instrument pointing. (panel b): time series of differences (%) between LP and MLS for versions 2.5 (red) and 2.6 (black). Dashed/dotted color lines show linear fits to differences.

versions exhibit positive biases relative to MLS on the order of 3%–6% between 32 and 40 km, and negative biases above reaching −9% at ∼ 48 km. In version 2.6, biases with MLS decrease with increasing altitude above 48 km. The addition of three UV pairs and increased normalization altitude (from 55.5 to 60.5 km) in version 2.6 have resulted in the extension of the upper limit of LP retrievals to 57.5 km. The increased number of wavelengths and dynamic range, where each UV pair is used by the algorithm, have also helped to reduce the oscillations seen in version 2.5 (Kramarova et al., 2018) at altitudes around 37.5 and 43.5 km, where the version 2.5 algorithm transitions between three pairs, and which are more evident in the Southern Hemisphere.

The differences between the two LP versions are larger in the lower part of the ozone profiles below 31 km, where LP retrievals primarily rely on the VIS triplet (see Figure 8). There are many factors that contribute to this, including changes in the ozone-sensitive wavelength in the VIS triplet (from 600 to 606 nm), aerosol particle size distributions, altitude registration and the stray light correction. UV and VIS measurements are blended in the version 2.6 algorithm to provide a smoother transition between 28 and 32 km. This effect is more pronounced in the North Hemisphere, where version 2.5 shows strong negative biases between 25 and 30 km, as noted in the previous study (Kramarova et al., 2018). These negative biases are still present in version 2.6 but with a smaller magnitude of about −3 to −6%. Around 20 km there is a vertical band with strong positive biases of about 5%–20% in version 2.6 that extends from the southern midlatitudes (∼40°S) to the northern polar latitudes that is not present in version 2.5. We found no changes in magnitude or structure of the mean biases as we extended the time record up to the end of 2023 (see Figure S11 in Supporting Information S1).

Another way to compare the two LP versions is to evaluate changes in absolute biases against MLS between LP versions 2.5 and 2.6 (Figure 8c): $|O_3^{LP2.5} - O_3^{MLS}| - |O_3^{LP2.6} - O_3^{MLS}|$ Positive biases (reddish colors) in Figure 8c represent places where LP version 2.5 has larger absolute biases against MLS compared to version 2.6, and therefore these are the places where the absolute biases decreased in LP version 2.6. Noticeable improvements (>∼5%), as we noted before, can be seen in the Northern Hemisphere between 25 and 30 km, in the lowermost stratosphere and above 50 km. But absolute biases increased in version 2.6 by more than 5% at 20 km from 40°S to 70°N, between 25 and 20 km in the southern mid-latitudes 50°S–70°S and in the equatorial upper troposphere.

To investigate the stability of the LP record, we analyzed the MLS and LP ozone time series at each latitude and altitude grid (Figures 9 and 10). Previously, in version 2.5, we found a significant upward drift at altitudes above

10.1029/2024EA003707

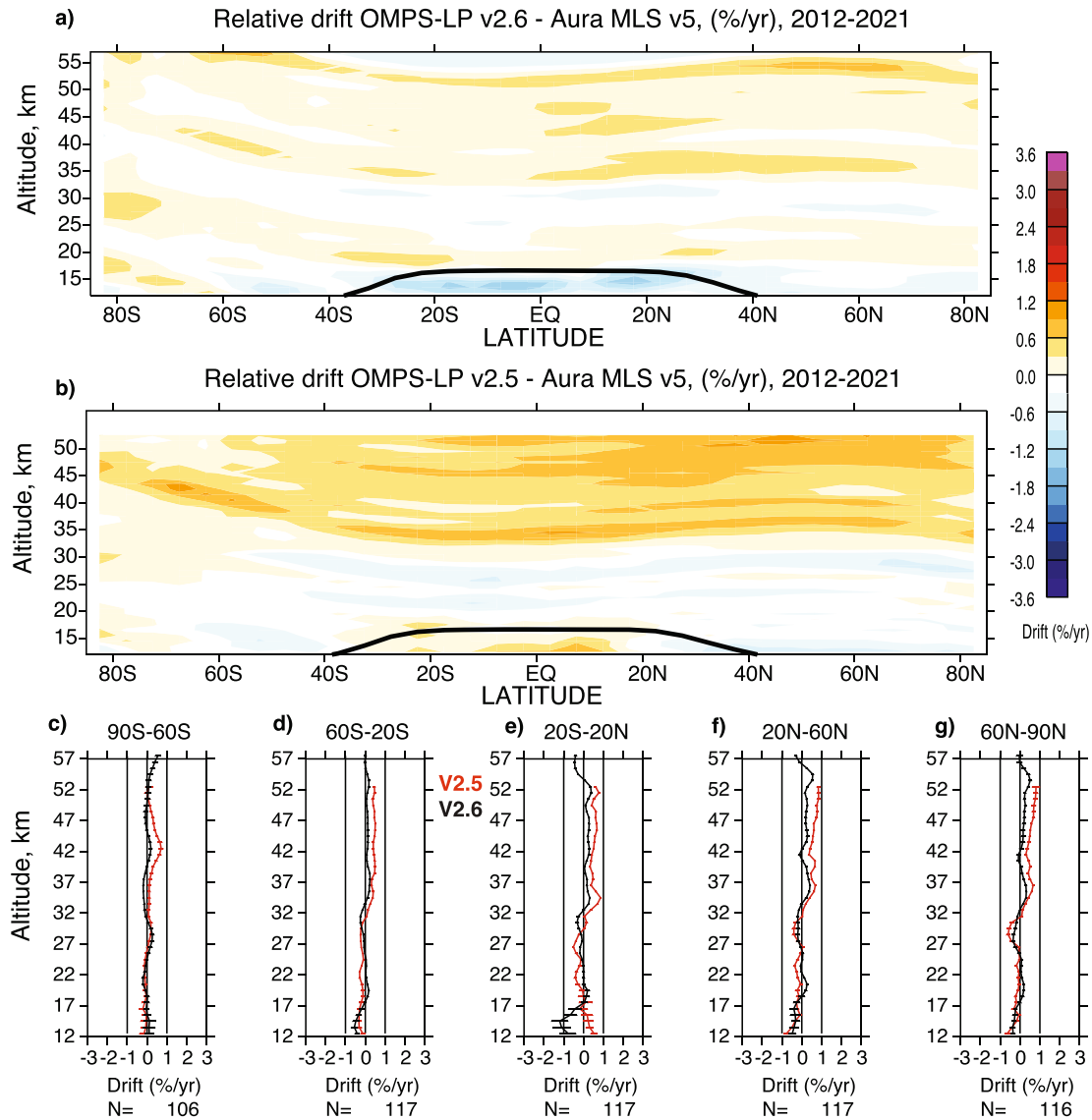

Figure 10. Panel (a) relative drift between OMPS LP version 2.6 and MLS version 5 over almost 10 years from April 2012 through December 2021 as a function of altitude and latitude (5° latitude grid). Solid black line shows the mean tropopause height. Panel (b) is the same as panel (a) but for OMPS LP v2.5. Panels (c–g) show vertical structures of the relative drift in 5 wide latitude bins for versions 2.5 (red lines) and 2.6 (black lines). Horizontal error bars show 1σ errors for the linear fit. Numbers on the bottom indicate the number of months in each of the five bins.

35 km, where ozone retrievals are very sensitive to the accuracy and stability of the instrument pointing. We found that the version 2.6 LP record is more stable, and compares better with MLS. Differences between MLS and version 2.6 are smaller in 2012 by ~2% compared to differences with version 2.5. The relative drift against MLS has reduced from 5% per decade (±0.4% per decade) in version 2.5 to 2.1% per decade (±0.4% per decade) in version 2.6. There is a small upward drift between LP version 2.6 and MLS in early years between 2012 and 2018 (Figure 9), but after that there is no obvious drift. We believe that the removal of the second 0.1-km step in altitude registration in September 2014, and the time-dependent spectral shift corrections are responsible for the observed improvements (see Section 2.2.1). The mean negative offset is also smaller between version 2.6 and MLS, mostly due to the changes in the earlier part of the record (Figure 9b).

We estimated the relative drift between LP and MLS by simply fitting a linear trend to the monthly zonal mean differences (Figures 9b and 10). In version 2.5, the vertical pattern in the relative drift (Figure 10b) was consistent with a possible drift in altitude registration: the drift is predominantly positive above the ozone peak and negative

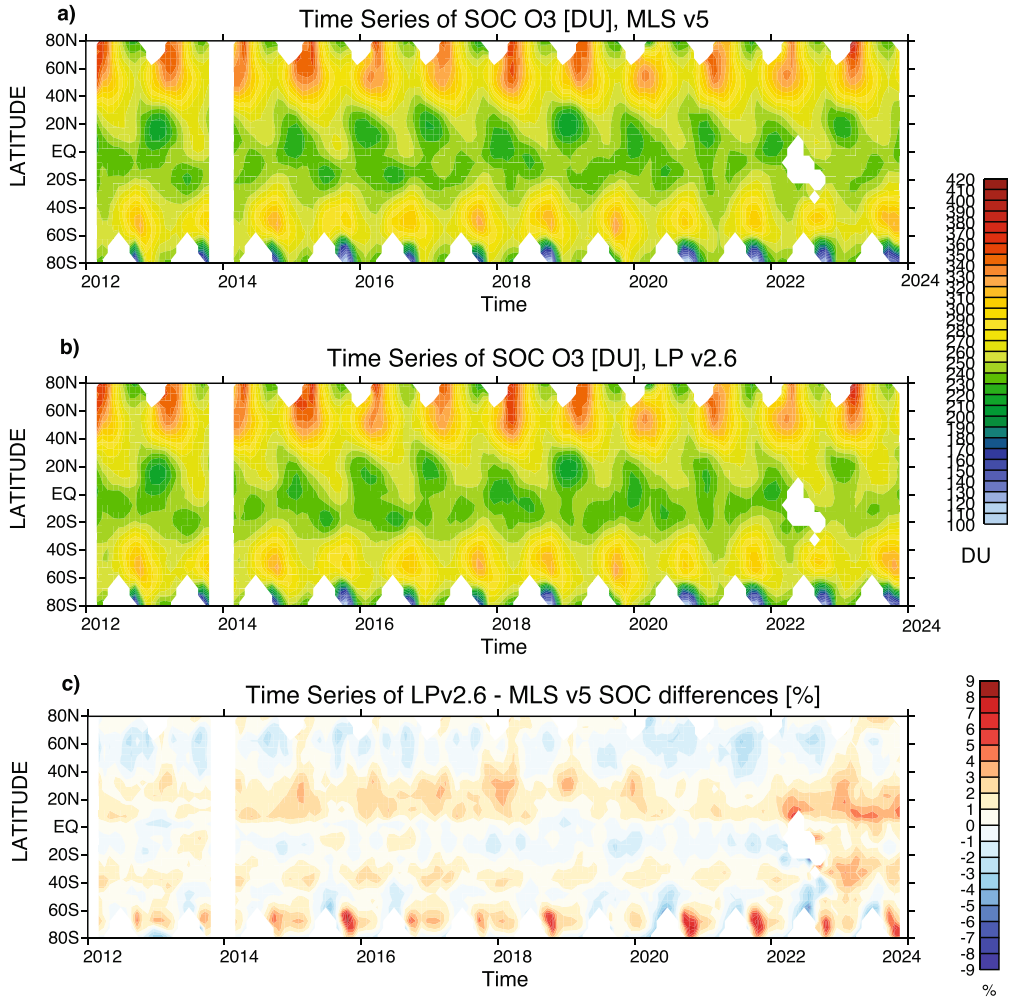

Figure 11. Time series of monthly zonal mean stratospheric ozone columns in DU derived from MLS version 5 (a) and OMPS LP version 2.6 (b) shown as a function of latitude and time. Stratospheric columns are integrated between 12.5 km or cloud top and 57.5 km. Panel (c) shows differences in % between LP and MLS.

below. We found that the pattern is very different in version 2.6 (Figure 10a). Overall, we see a substantial reduction in the magnitude of the drift, making the version 2.6 record more suitable for the ozone trend studies. While the drift between LP version 2.6 and MLS is still predominantly positive in the upper stratosphere, the magnitude has reduced to about 0.2% per year (or 2% per decade) or less. We found that the relative drift decreases in the upper stratosphere if we extend the considered time period by two more years to the end of 2023 (see Figure S12 in Supporting Information S1). In the middle stratosphere between 25 and 35 km the drift is slightly negative. We also see a strong negative relative drift in the upper equatorial troposphere up to −10% per decade while it was positive in version 2.5. Though the record extension reduces the drift in the upper stratosphere, the drift in the southern subtropics (20°S–40°S) between 15 and 21 km (see Figure S12 in Supporting Information S1) sharply increases suggesting that LP retrievals overestimate ozone concentrations after the Hunga eruption in that region.

Finally, we consider the time series of stratospheric ozone columns (SOC) between 12.5 and 57.5 km (Figure 11). If LP ozone profiles were truncated because of the presence of clouds, we cut the matching MLS profile as well and integrate profiles down to the lowest available level. However, we require the minimum number of levels in the profile to be equal to 40 (corresponds to 18.5–57.5 km). After the Hunga eruption we filtered LP profiles leading to a gap in the SOC record in the equatorial latitudes. Both LP and MLS show similar latitudinal and seasonal patterns in the SOC distribution suggesting that LP ozone can be used to extend MLS record into the future for many applications. The differences range mostly to within ±2% but there are clear latitudinal and

seasonal patterns. The largest seasonal variations are observed over the southern polar latitudes, with a strong positive bias observed during austral spring. It is outside of the scope of this study to analyze seasonal differences, but this topic will be considered in the upcoming comprehensive validation paper where OMPS LP will be compared with an extended set of correlative satellite and ground-based observations. The differences in SOC increase in the last 2 years and become predominantly positive in the tropics and mid-latitudes. The increases in mean differences in 2022–2023 are more apparent at altitudes near the ozone peak between 22 and 26 km (see Figure S13 in Supporting Information S1). The Hunga eruption increased concentration of water vapor in the stratosphere globally (e.g., Millán et al., 2022), but the LP wavelengths used by the retrieval algorithm are not sensitive to water vapor absorption. Further investigation is needed to understand these changes and any potential links to the Hunga eruption.

4. Conclusions

In this study we described the new version (version 2.6) of the OMPS LP ozone profile data set. This data set includes incremental improvements in calibration, retrieval algorithm, and data quality compared to the previous version 2.5. OMPS LP provides ozone profiles with a high vertical resolution and dense spatial sampling, offering an adequate alternative for extending the MLS ozone record into the future for many applications. We described changes in calibration applied to measured limb-scattered radiances and modifications implemented in the retrieval algorithm.

Calibration updates that affected ozone retrievals include improvements in the stray light model, radiometric calibration, the wavelength shift correction and altitude registration. As a result of updates in altitude registration, the RSAS technique, applied to the time period between April 2012 and December 2021, demonstrated improvements in the stability of the version 2.6 record with no apparent trends.

The LP retrieval algorithm was also modified in version 2.6. Following recommendations provided in the scientific literature, we replaced outdated algorithmic parameters such as the ozone and nitrogen dioxide absorption cross-sections and climatologies. Though these updates yield very small systematic (less than ±1–2%) changes in ozone retrievals, it is important to use the best available parameters. In addition, we replaced the particle size distribution model for stratospheric aerosols. We now use the gamma-function model to retrieve aerosol extinction from the same limb measurements at 675 nm which are then used to correct for the aerosol contamination in the ozone retrieval algorithm. We estimated the sensitivity of the algorithm to changes in the assumed particle size distribution and show that the largest changes, up to 30%–35%, are seen in the tropical (20°S–20°N) upper troposphere (12.5–15.5 km), where the aerosol concentration is typically higher and the LP sensitivity to ozone is low. In the middle stratosphere (18.5–30.5 km), the ozone algorithm is more sensitive to changes in the aerosol model in the Northern Hemisphere because of the forward scattering geometry of the LP observations. The changes in the aerosol model there can produce up to ±2–7% error in retrieved ozone.

The largest algorithmic change in version 2.6 is that we combine UV and VIS measurements and retrieve a single merged ozone profile between 12.5 and 57.5 km. We also increased the number of UV pairs to 6, increased the normalization altitude for UV radiances to 60.5 km, limited the vertical range where each UV pair contributes based on sensitivity to ozone, and employed Tikhanov's regularization. We found that the averaging kernels are more consistent throughout the entire profile in terms of the peak magnitude and the width. This means that the version 2.6 algorithm is better optimized for keeping a uniform sensitivity throughout the entire vertical range with the resolution of ∼1.9–2.5 km. The vertical resolution quickly degrades in the tropics below the ozone peak and decreases to 4–10 km between 12.5 and 17.5 km in the tropical upper troposphere. The retrieval precision, reported with each profile, has reduced by a factor of two compared to version 2.5 and ranges between 3% and 4% in the middle stratosphere. The accuracy of LP retrieved ozone profiles depends on many factors, and we report a set of quality flags to help users identify and exclude lower quality data. In this study, we introduced each flag and analyzed their spatial and temporal distribution.

We compared the OMPS LP record with Aura MLS and found incremental improvements in version 2.6. The algorithm modifications helped to reduce vertical oscillations seen in the previous version, particularly near altitudes where the algorithm switches wavelengths. Negative biases above 45 km have been reduced in version 2.6. Because UV and VIS radiances are merged in the middle stratosphere, version 2.6 enables a smoother transition in the altitude range between 28 and 33 km. Mean biases with MLS are within ±10% above 20 km and in many places are less than ±5%.

The most notable improvement in version 2.6 is the reduction in relative drifts between LP and MLS. Particularly, in the upper stratosphere above 35 km—the region most sensitive to error in altitude registration—the relative drift between LP version 2.6 and MLS is around or less than 2% per decade (vs. 5%–10% per decade for LP 2.5—MLS).

We introduced a filter based on retrieved aerosol extinction to remove ozone profiles affected by the Hunga eruption in the lower stratosphere (below 24.5 km). As a result of the filtering, there are gaps in OMPS LP observations in the lower stratosphere between 12.5 and 22.5 km in the southern midlatitudes and tropics (45°S–20°N) that last for several months following the eruption. We see an increase in differences between LP and MLS in 2022–2023 compared to the previous 10 years. Further investigation is needed to determine if the 2022–2023 increase is related to the elevated stratospheric aerosol load due to the Hunga eruption.

Overall, the findings of this study demonstrate the importance of continuous improvements in instrument calibration and retrieval algorithms to ensure high accuracy and stability of satellite ozone measurements. Periodic evaluation of the LP ozone data sets, and comparisons with independent measurements, are critical for determining the reliability and fitness of the LP data for various scientific applications.

Data Availability Statement

Suomi OMPS LP version 2.6 (Kramarova, 2023) and Aura MLS version 5 (Schwartz et al., 2021) ozone data are publically available at the Goddard Earth Sciences Data and Information Services Center (GES DISC).

Acknowledgments
Authors are grateful to the MLS Team at NASA JPL for producing a consistent high-quality ozone data set. Authors would like to thank Didier Rault for developing the original ozone retrieval algorithm for the OMPS LP. We also would like to thank Robert Loughman for maintaining the radiative transfer code for the OMPS LP. We are grateful to all members of the OMPS Team for their work supporting the OMPS mission. This work was funded under the NASA project 20-SNPPSP20-0019 "Synergistic use of Limb and Nadir Measurements to continue the NASA Standard Ozone Products from OMPS on Suomi NPP and NOAA-20." SD and YJ were supported by a NOAA JPSS Proving Ground and Risk Reduction Program grant. Authors would like to thank Nigel Richards for constructive comments.

References

Arosio, C., Chipperfield, M. P., Rozanov, A., Weber, M., Dhomse, S., Feng, W., et al. (2024). Investigating zonal asymmetries in stratospheric ozone trends from satellite limb observations and a chemical transport model. *Journal of Geophysical Research: Atmospheres*, *129*(8), e2023JD040353. https://doi.org/10.1029/2023JD040353

Arosio, C., Rozanov, A., Gorshelev, V., Laeng, A., & Burrows, J. P. (2022). Assessment of the error budget for stratospheric ozone profiles retrieved from OMPS limb scatter measurements. *Atmospheric Measurement Techniques*, *15*(20), 5949–5967. https://doi.org/10.5194/amt-15-5949-2022

Bass, A. M., & Paur, R. J. (1985). The ultraviolet cross-sections of ozone: I. The measurements. In C. S. Zerefos & A. Ghazi (Eds.), *Atmospheric ozone* (pp. 606–616). Springer. https://doi.org/10.1007/978-94-009-5313-0_120

Brion, J., Chakir, A., Daumont, D., Malicet, J., & Parisse, C. (1993). High resolution laboratory absorption cross-section of O_3. Temperature effect. *Chemical Physics Letters*, *213*(5–6), 610–612. https://doi.org/10.1016/0009-2614(93)89169-I

Brohede, S. M., Haley, C. S., Mclinden, C. A., Sioris, C. E., Murtagh, D. P., Petelina, S. V., et al. (2007). Validation of Odin/OSIRIS stratospheric NO_2 profiles. *Journal of Geophysical Research*, *112*(D7), D07310. https://doi.org/10.1029/2006JD007586

Burkholder, J. B., & Talukdar, R. K. (1994). Temperature dependence of the ozone absorption spectrum over the wavelength range 410 to 760 nm. *Geophysical Research Letters*, *21*(7), 581–584. https://doi.org/10.1029/93GL02311

Chen, Z., Bhartia, P. K., Loughman, R., Colarco, P., & DeLand, M. (2018). Improvement of stratospheric aerosol extinction retrieval from OMPS/LP using a new aerosol model. *Atmospheric Measurement Techniques*, *11*(12), 6495–6509. https://doi.org/10.5194/amt-11-6495-2018

Chen, Z., DeLand, M., & Bhartia, P. K. (2016). A new algorithm for detecting cloud height using OMPS/LP measurements. *Atmospheric Measurement Techniques*, *9*(3), 1239–1246. https://doi.org/10.5194/amt-9-1239-2016

Degenstein, D. A., Bourassa, A. E., Roth, C. Z., & Llewellyn, E. J. (2009). Limb scatter ozone retrieval from 10 to 60 km using a multiplicative algebraic reconstruction technique. *Atmospheric Chemistry and Physics*, *9*(17), 6521–6529. https://doi.org/10.5194/acp-9-6521-2009

DeLand, M. T., & Gorkavyi, N. (2020). PMC observations from the OMPS Limb Profiler. *Journal of Atmospheric and Solar-Terrestrial Physics*, *213*, 105505. https://doi.org/10.1016/j.jastp.2020.105505

Farman, J. C., Gardiner, B. G., & Shanklin, J. D. (1985). Large losses of ozone in Antarctica reveal seasonal ClO_x/NO_x interaction. *Nature*, *315*(6016), 207–210. https://doi.org/10.1038/315207a0

Fisher, B. L., Lamsal, L. N., Fasnacht, Z., Oman, L. D., Joiner, J., Krotkov, N. A., et al. (2024). Revised estimates of NO_2 reductions during the COVID-19 lockdowns using updated TROPOMI NO_2 retrievals and model simulations. *Atmospheric Environment*, *326*, 120459. https://doi.org/10.1016/j.atmosenv.2024.120459

Flittner, D. E., Bhartia, P. K., & Herman, B. M. (2000). O_3 profiles retrieved from limb scatter measurements: Theory. *Geophysical Research Letters*, *27*(17), 2601–2604. https://doi.org/10.1029/1999GL011343

Flynn, L. E., Seftor, C. J., Larsen, J. C., & Xu, P. (2006). The ozone mapping and profiler suite. In J. J. Qu, W. Gao, M. Kafatos, R. E. Murphy, & V. V. Salomonson (Eds.), *Earth science satellite remote sensing* (pp. 279–296). Springer. https://doi.org/10.1007/978-3-540-37293-6_15

Gelaro, R., McCarty, W., Suárez, M. J., Todling, R., Molod, A., Takacs, L., et al. (2017). The modern-era retrospective analysis for research and applications, version 2 (MERRA-2). *Journal of Climate*, *30*(14), 5419–5454. https://doi.org/10.1175/JCLI-D-16-0758.1

Gorshelev, V., Serdyuchenko, A., Weber, M., Chehade, W., & Burrows, J. P. (2014). High spectral resolution ozone absorption cross-sections—Part 1: Measurements, data analysis and comparison with previous measurements around 293 K. *Atmospheric Measurement Techniques*, *7*(2), 609–624. https://doi.org/10.5194/amt-7-609-2014

Herman, B. M., Ben-David, A., & Thome, K. J. (1994). Numerical techniques for solving the radiative transfer equation for a spherical shell atmosphere. *Applied Optics*, *33*(9), 1760–1770. https://doi.org/10.1364/AO.33.001760

Janz, S. J., Hilsenrath, E., Flittner, D. E., & Heath, D. F. (1996). Rayleigh scattering attitude sensor. In *Proceedings of SPIE 2831, Atmospheric Ultraviolet and Space Remote Sensing: Methods and Instrumentation* (Vol. 146). https://doi.org/10.1117/12.257207

Jaross, G., Bhartia, P. K., Chen, G., Kowitt, M., Haken, M., Chen, Z., et al. (2014). OMPS Limb Profiler instrument performance assessment. *Journal of Geophysical Research: Atmospheres*, *119*(7), 4399–4412. https://doi.org/10.1002/2013JD020482

Kramarova, N. A. (2023). OMPS-NPP L2 LP ozone (O3) vertical profile swath daily center slit V2.6 [Dataset]. *NASA Goddard Earth Sciences Data and Information Services Center*. https://doi.org/10.5067/8MO7DEDYTBH7

Kramarova, N. A., Bhartia, P. K., Jaross, G., Moy, L., Xu, P., Chen, Z., et al. (2018). Validation of ozone profile retrievals derived from the OMPS LP version 2.5 algorithm against correlative satellite measurements. *Atmospheric Measurement Techniques*, *11*(5), 2837–2861. https://doi.org/10.5194/amt-11-2837-2018

Kramarova, N. A., & DeLand, M. (2023). *README document for the Suomi-NPP OMPS LP L2 O3 daily product (version 2.6)* (p. 36). Goddard Earth Sciences Data and Information Services Center (GES DISC). Retrieved from https://disc.gsfc.nasa.gov/datasets/OMPS_NPP_LP_L2_O3_DAILY_2.6/summary?keywords=OMPS

Kramarova, N. A., Nash, E. R., Newman, P. A., Bhartia, P. K., McPeters, R. D., Rault, D. F., et al. (2014). Measuring the Antarctic ozone hole with the new ozone mapping and profiler suite (OMPS). *Atmospheric Chemistry and Physics*, *14*(5), 2353–2361. https://doi.org/10.5194/acp-14-2353-2014

Livesey, N. J., Read, W. G., Wagner, P. A., Froidevaux, L., Santee, M. L., Schwartz, M. J., et al. (2022). *Version 5.0x Level 2 and 3 data quality and description document* (Tech. Rep. No. JPL D-105336 Rev. B). Jet Propulsion Laboratory. Retrieved from https://mls.jpl.nasa.gov/data/v5-0_data_quality_document.pdf

Livesey, N. J., Snyder, W. V., Read, W. G., & Wagner, P. A. (2006). Retrieval algorithms for the EOS microwave limb sounder (MLS). *IEEE Transactions on Geoscience and Remote Sensing*, *44*(5), 1144–1155. https://doi.org/10.1109/TGRS.2006.872327

Loughman, R. P., Bhartia, P. K., Chen, Z., Xu, P., Nyaku, E., & Taha, G. (2018). The ozone mapping and profiler suite (OMPS) limb profiler (LP) version 1 aerosol extinction retrieval algorithm: Theoretical basis. *Atmospheric Measurement Techniques*, *11*(5), 2633–2651. https://doi.org/10.5194/amt-11-2633-2018

Loughman, R. P., Flittner, D., Nyaku, E., & Bhartia, P. K. (2015). Gauss-Seidel limb scattering (GSLS) radiative transfer model development in support of the ozone mapping and profiler suite (OMPS) limb profiler mission. *Atmospheric Chemistry and Physics*, *15*(6), 3007–3020. https://doi.org/10.5194/acp-15-3007-2015

Loughman, R. P., Flittner, D. E., Herman, B. M., Bhartia, P. K., Hilsenrath, E., & McPeters, R. D. (2005). Description and sensitivity analysis of a limb scattering ozone retrieval algorithm. *Journal of Geophysical Research*, *110*(D19), D19301. https://doi.org/10.1029/2004JD005429

Lucchesi, R. (2013). *File specification for GEOS-5 FP-IT* (p. 60). GMAO Office Note No. 2 (Version 1.2). Retrieved from http://gmao.gsfc.nasa.gov/pubs/office_notes

McPeters, R. D., Janz, S. J., Hilsenrath, E., Brown, T. L., Flittner, D. E., & Heath, D. F. (2000). The retrieval of O_3 profiles from limb scatter measurements: Results from the shuttle ozone limb sounding experiment. *Geophysical Research Letters*, *27*(17), 2597–2600. https://doi.org/10.1029/1999GL011342

McPeters, R. D., & Labow, G. J. (2012). Climatology 2011: An MLS and Sonde derived ozone climatology for satellite retrieval algorithms. *Journal of Geophysical Research*, *117*(10), D10303. https://doi.org/10.1029/2011JD017006

Mérienne, M. F., Jenouvier, A., & Coquart, B. (1995). The NO_2 absorption spectrum. I: Absorption cross-sections at ambient temperature in the 300–500 nm region. *Journal of Atmospheric Chemistry*, *20*(3), 281–297. https://doi.org/10.1007/BF00694498

Millán, L., Santee, M. L., Lambert, A., Livesey, N. J., Werner, F., Schwartz, M. J., et al. (2022). The Hunga Tonga-Hunga Ha'apai hydration of the stratosphere. *Geophysical Research Letters*, *49*(13), e2022GL099381. https://doi.org/10.1029/2022GL099381

Moy, L., Bhartia, P. K., Jaross, G., Loughman, R., Kramarova, N., Chen, Z., et al. (2017). Altitude registration of limb-scattered radiation. *Atmospheric Measurement Techniques*, *10*(1), 167–178. https://doi.org/10.5194/amt-10-167-2017

NASA. (2023). NASA's terra, aqua, and aura data continuity workshop, workshop summary. Retrieved from https://nspires.nasaprs.com/external/viewrepositorydocument/cmdocumentid=985170/solicitationId=%7BEC26B6F5-5B02-8932-45F4-EAF5DED2DA14%7D/viewSolicitationDocument=1/Terra-Aqua-Aura-Data-Continuity-RFI-and-Workshop-Summary2.pdf

Nielsen, J. E., Pawson, S., Molod, A., Auer, B., da Silva, A. M., Douglass, A. R., et al. (2017). Chemical mechanisms and their applications in the Goddard Earth Observing System (GEOS) earth system model. *Journal of Advances in Modeling Earth Systems*, *9*(8), 3019–3044. https://doi.org/10.1002/2017MS001011

Orbe, C., Oman, L. D., Strahan, S. E., Waugh, D. W., Pawson, S., Takacs, L. L., & Molod, A. M. (2017). Large-scale atmospheric transport in GEOS replay simulations. *Journal of Advances in Modeling Earth Systems*, *9*(7), 2545–2560. https://doi.org/10.1002/2017MS001053

Prather, M., & Jaffe, A. H. (1990). Global impact of the Antarctic ozone hole: Chemical propagation. *Journal of Geophysical Research*, *95*(D4), 3473–3492. https://doi.org/10.1029/JD095iD04p03473

Rault, D. F. (2005). Ozone profile retrieval from Stratospheric Aerosol and Gas Experiment (SAGE III) limb scattering measurements. *Journal of Geophysical Research*, *110*(D9), D09309. https://doi.org/10.1029/2004JD004970

Rault, D. F., & Loughman, R. P. (2013). The OMPS limb profiler environmental data record algorithm theoretical basis document and expected performance. *IEEE Transactions on Geoscience and Remote Sensing*, *51*(5), 2505–2527. https://doi.org/10.1109/TGRS.2012.2213093

Rodgers, C. D. (2000). *Inverse methods for atmospheric sounding: Theory and practice* (p. 238). World Scientific.

Schoeberl, M. R., Wang, Y., Ueyama, R., Taha, G., & Yu, W. (2023). The cross equatorial transport of the Hunga Tonga-Hunga Ha'apai eruption plume. *Geophysical Research Letters*, *50*(4), e2022GL102443. https://doi.org/10.1029/2022GL102443

Schwartz, M., Froidevaux, L., Livesey, N., Read, W., & Fuller, R. (2021). MLS/Aura level 3 daily binned ozone (O3) mixing ratio on assorted grids V005 [Dataset]. *NASA Goddard Earth Sciences Data and Information Services Center*. https://doi.org/10.5067/AURA/MLS/DATA/3516

Stolarski, R. S., Krueger, A. J., Schoeberl, M. R., McPeters, R. D., Newman, P. A., & Alpert, J. C. (1986). Nimbus 7 satellite measurements of the springtime Antarctic ozone decrease. *Nature*, *322*(6082), 808–811. https://doi.org/10.1038/322808a0

Taha, G., Jaross, G., Fussen, D., Vanhellemont, F., Kyrölä, E., & McPeters, R. D. (2008). Ozone profile retrieval from GOMOS limb scattering measurements. *Journal of Geophysical Research*, *113*(D23), D23307. https://doi.org/10.1029/2007JD009409

Taha, G., Loughman, R., Colarco, P. R., Zhu, T., Thomason, L. W., & Jaross, G. (2022). Tracking the 2022 Hunga Tonga-Hunga Ha'apai aerosol cloud in the upper and middle stratosphere using space-based observations. *Geophysical Research Letters*, *49*(19), e2022GL100091. https://doi.org/10.1029/2022GL100091

Vandaele, A. C., Hermans, C., Simon, P. C., Carleer, M., Colin, R., Fally, S., et al. (1998). Measurements of the NO_2 absorption cross-section from 42 000 cm^{-1} to 10 000 cm^{-1} (238–1000 nm) at 220 K and 294 K. *Journal of Quantitative Spectroscopy and Radiative Transfer*, *59*(3–5), 171–184. https://doi.org/10.1016/S0022-4073(97)00168-4

von Clarmann, T., Degenstein, D. A., Livesey, N. J., Bender, S., Braverman, A., Butz, A., et. al. (2020). Overview: Estimating and reporting uncertainties in remotely sensed atmospheric composition and temperature. *Atmospheric Measurement Techniques*, *13*(8), 4393–4436. https://doi.org/10.5194/amt-13-4393-2020

Wargan, K., Kramarova, N., Weir, B., Pawson, S., & Davis, S. M. (2020). Toward a reanalysis of stratospheric ozone for trend studies: Assimilation of the Aura microwave limb sounder and ozone mapping and profiler suite limb profiler data. *Journal of Geophysical Research: Atmospheres*, *125*(4), e2019JD031892. https://doi.org/10.1029/2019JD031892

WMO (World Meteorological Organization). (2022). *Scientific assessment of ozone depletion: 2022* (GAW report No. 278) (p. 509). WMO. Retrieved from https://ozone.unep.org/science/assessment/sap

Xu, P. Q., Bhartia, P. K., Jaross, G. J., DeLand, M. T., Larsen, J. C., Fleig, A., et al. (2014). Release 2 data products from the ozone mapping and profiling suite (OMPS) limb profiler. In *Proceedings of SPIE 9242, Remote Sensing of Clouds and the Atmosphere XIX; and Optics in Atmospheric Propagation and Adaptive Systems* (Vol. XVII, pp. 92420K). https://doi.org/10.1117/12.2067320

Ziemke, J. R., Labow, G. J., Kramarova, N. A., McPeters, R. D., Bhartia, P. K., Oman, L. D., et al. (2021). A global ozone profile climatology for satellite retrieval algorithms based on Aura MLS measurements and the MERRA-2 GMI simulation. *Atmospheric Measurement Techniques*, *14*(10), 6407–6418. https://doi.org/10.5194/amt-14-6407-2021